Available online at www.sciencedirect.com
ScienceDirect
Journal of Power Sources 159 (2006) 1428–1439
JOURNAL OF POWER SOURCES
www.elsevier.com/locate/jpowsour

The impedance characteristics of Mars Exploration Rover Li-ion batteries

B.V. Ratnakumar*, M.C. Smart, L.D. Whitcanack, R.C. Ewell

Jet Propulsion Laboratory, California Institute of Technology, 4800 Oak Grove Drive, Pasadena, CA 91109, United States

Received 15 October 2005; received in revised form 24 November 2005; accepted 25 November 2005
Available online 24 January 2006

Abstract

Determination of the cell or battery impedance is critical to predicting and managing the battery performance, especially in a remote application such as in a spacecraft. While electrochemical impedance spectroscopy provides more quantitative and diverse information on the electrochemical processes, it is less informative in the absence of a reference electrode and/or more cumbersome in multi-cell batteries. DC impedance values, on the other hand, are relatively easy to implement and with subtle variations in the pulse conditions, i.e., pulse magnitude and pulse width, may provide useful trends in the ohmic, charge transfer and mass transfer components. In order to assess the impedance values of the Li-ion cells and batteries and their impact on the current-limiting series resistors in the Mars Exploration Rovers (MER), we, therefore, adopted DC methods under a variety of test conditions, i.e., magnitude and duration of the sampling current pulses, states of charge of the cells and batteries, as well as at different (low) temperatures. Understandably, higher current pluses tend to lower the contribution from the charge transfer, while longer pulses result in a higher share of the diffusional component in the overall impedance. Based on relatively simple analyses, we derived useful trends for the ohmic, charge transfer and mass transfer components of the cell impedance, as a function of temperature and obtained activation energies for these processes. Finally, these measurements assisted us in the assessment of risk associated with the series resistors during the launching of the Mars Rover missions.

Keywords: Lithium-ion batteries; Mars Rovers; DC impedance; Low temperature

1. Introduction

The impedance, or the internal resistance, of a battery may be understood simply as the resistance offered by the battery to the flow of (discharge) current through it. However, due to its dynamic nature with respect to current and time, it is rather difficult to attribute a unique value for the battery impedance, which the power subsystem analysts often desire. It is a strong function of the method of determination as well as the measurement conditions, and this dependence is specific to each battery system. Other experimental conditions have considerable impact on battery impedance including temperature, state of charge, and history of the cell/battery.

In this paper, we address the multi-dimensional aspects of cell and battery impedance, specifically those of lithium-ion cells and batteries developed for NASA's Mars Exploration Rovers. The energy source on the Mars Rovers is comprised of deployable solar arrays with triple-junction GaInP/GaAs/Ge cells. For augmenting this power source and to support nighttime experiments during geological and mineralogical studies on the surface of Mars, the rovers use rechargeable lithium-ion batteries, which are described in detail in our previous publications [1–3].

Briefly, the lithium-ion rechargeable battery system provides several unique characteristics, important for both the Spirit and Opportunity rovers. Specifically, the battery system provides adequate power and energy for the missions, within the constraints of mass and volume, due to its high specific energy and energy density. Furthermore, the Li-ion battery contains a low temperature electrolyte developed at JPL, i.e., 1 M $LiPF_6$ dissolved in an equi-proportion ternary mixture of ethylene carbonate, dimethyl carbonate and diethyl carbonate [4]. This electrolyte enabled operations at sub-zero temperatures, down to −30 °C, thus making the thermal management of the battery considerably easier [5]. These batteries are located in the aerogel-insulated warm electronics box for thermal purposes. Using a combination of resistive heaters, radioisotope heating

* Corresponding author. Tel.: +1 818 354 0110; fax: +1 818 393 6951.
E-mail address: ratnakumar.v.bugga@jpl.nasa.gov (B.V. Ratnakumar).

0378-7753/$ – see front matter © 2006 Published by Elsevier B.V.
doi:10.1016/j.jpowsour.2005.11.085

units (RHUs) and a paraffin-thermal-switch-activated passive heat rejection system, the rover batteries are maintained between −20 and +30 °C.

From the mission perspective, the rover lithium-ion batteries were designed to provide: (1) 24–36 V in all phases, (2) 200 Wh during launch, (3) about 160 Wh during cruise for supporting potential anomalies during trajectory control maneuvers and (4) about 283 Wh for surface operations, for about 300 cycles over 90 sols for the primary mission. In addition, each of the rover batteries was designed to provide energy to fire three simultaneous squibs (each with a nominal load of 7 A and a maximum duration of 32 mS) with an interval of at least 100 ms. To meet the above requirements, each of the rovers has two parallel lithium-ion batteries, each with eight 10 Ah cells in series.

During squib-firing tests with the flight spacecraft, all three squibs in series with the battery experienced a plasma short to ground, which let significant current (15–30 A) flow through the chassis of the spacecraft back to the battery, thus blowing a 5 A fuse located between the chassis and the battery. The current-limiting resistor in series with each of squibs and the rover battery assembly unit could have become thermally stressed, if high currents were allowed to pass through it.

For an assessment of the health of the current-limiting resistors, and hence the spacecraft, it was essential to make an analysis of the maximum current that could flow through the current-limiting resistors in the squib plasma shorting condition. In other words, it was critical to estimate the rover battery impedance under the prevailing conditions. From this standpoint, a higher value for the battery impedance is desirable (about 400 mΩ at −16 °C). This estimate of battery impedance was critical in order to determine whether the current limiting resistors were overstressed and needed to be replaced prior to launch. For a proper risk assessment prior to launch, we performed several systematic measurements on the impedance of MER Li-ion cells and batteries, as reported here. In addition, systematic measurements were made on the cells at different temperatures and states of charge, using current pulses of different magnitude and pulse width to derive trends in the ohmic, charge transfer and mass transfer components.

2. Electrochemical description of impedance

The cell or battery voltage is suppressed during discharge as a result of its impedance, consisting of three different types, as represented below

$$E = E_{OC} - \eta_{ohmic} - \eta_{Ch.Tr} - \eta_{diff} \quad (1)$$

where E is the voltage under load, E_{OC} the open-circuit voltage, η_{ohmic} the ohmic polarization resulting from the ionic resistance of the electrolyte and electronic resistance of the electrodes and leads, $\eta_{Ch.Tr}$ the charge transfer or activation polarization of the slower or rate-determining process in the anodic (or cathodic) reaction, and η_{diff} is the diffusion polarization corresponding to slow mass transfer of either reactants or products in one of the electrodes, once again the rate-determining electrode. Here, diffusion is assumed to be the dominant mode of mass transfer, which is quite likely with lithium-ion cells, due to slow diffusional rates of lithium ions in the lattice of the intercalating electrodes. Out of these three polarizations, the ohmic polarization, being a product of current and ohmic resistance, increases linearly with current, but is constant during the measurement. However, it may change marginally with the state of charge of the battery, mainly due to a change in the electronic resistance of the electrodes. Both charge transfer and diffusion polarizations are governed by the familiar electrochemical rate equation (or Butler–Volmer equation). This is expressed for the rate-determining electrochemical reaction as [6]:

$$\frac{i}{i_0} = \left\{ \left(\frac{C_O}{C_O^*} \right) \exp\left(-\frac{\alpha n F}{RT}(E - E_{equi}) \right) \right\} - \left\{ \left(\frac{C_R}{C_R^*} \right) \exp\left(\frac{(1-\alpha) n F}{RT}(E - E_{equi}) \right) \right\} \quad (2)$$

where i is the current density, i_0 the exchange current density of the reaction, α the cathodic energy transfer coefficient, n the number of electrons involved in the charge transfer process, E the applied electrode potential, E_{equi} the equilibrium electrode potential, C_O and C_R are the interfacial concentration of the oxidant and reductant species and C_O^* and C_R^* are the corresponding concentrations in the bulk of the electrodes, assuming the solid state diffusion of Li^+ is slower than in the electrolyte. Here, the charge transfer polarization is described by the exponential terms and the diffusional polarization is represented by the pre-exponential terms involving concentrations.

3. Experimental

3.1. Methods of impedance determination

The battery impedance can be determined either from AC methods or by DC polarization. The AC impedance has the advantage of being non-invasive, and gives a range of impedance values as a function of frequency, which, if analyzed properly, could be decomposed into contributions from ohmic, charge transfer and diffusion polarizations. This method requires a specialized set of instruments, including a potentiostat, lock-in amplifier or a frequency response analyzer. Such instruments are widely available for electrochemical impedance spectroscopy [7], along with relevant software to perform the experiment, as well as to aid in the data analyses. However, it is not possible to do such measurements on multi-cell batteries, because of the voltage limitation imposed by the potentiostat. In addition, the analysis of the data is not straightforward and requires sufficient understanding of the technique, underlying processes, as well as appropriate equivalent modeling circuits.

The DC impedance method, which involves a measurement of the voltage differential during either current-injection or current-interruption yields, on the other hand, a single value, which has more practical relevance. This method is often used in determining the cell and battery impedance during cycling and/or storage of lithium-ion cells and, thus, in estimating the performance degradation [8–10]. Between the DC impedance values measured during current-injection

and current-interruption, however, the current-injection method gives a slightly higher value compared to the current-interruption method in some cases, the difference coming mainly from the diffusion polarization. In terms of time scale, as the current is injected, the ohmic effects occur within microseconds range, followed by the capacitive (double layer capacitance charging) current in the mS range, followed by reaction polarization in the seconds range and diffusional polarization on extended discharge for multiples of seconds. Once the diffusional polarization sets in, the current-interruption method tends to give lower impedance value, unless a sufficient amount of time is allowed to elapse after current interruption, for a true equilibrium to be established and the concentration gradients are relaxed.

Based on these arguments, the difference between the current injection and current interruption should be related to the amplitude and width of the current pulse, which would determine the magnitude of concentration gradients, as well as temperature. In addition, during the pulse measurement, it is possible that the state of charge of the battery might change enough to alter the corresponding open circuit voltage and other characteristics. Lithium-ion cells have relatively sloping discharge curves compared to the nickel-based, aqueous systems, e.g., nickel–cadmium, nickel metal hydride or nickel–hydrogen batteries. If there is such a change in the state of charge, appropriate corrections need to be applied in the voltage, before calculating the impedance values.

3.2. Other experimental details

The test articles for this study include: (1) prismatic, 10 Ah lithium-ion cells and (2) 30 V, 8-Cell, 10 Ah Li-ion batteries, made for the Mars Exploration Rover (MER) project, by Yardney Technical Products (currently Lithion Inc.,) located in Pawcatuck, CT. The DC impedance measurements, as well as the charge–discharge operations, were carried out using a Maccor battery test system. Tenney environmental chambers were used to maintain the desired cell/battery temperatures, within ±1 °C.

4. Results

As mentioned above, we measured the impedance of the cells and batteries using DC current pulse methods, during current injection as well as current interruption.

4.1. DC current pulse impedance of 10 Ah Li-ion cells

The DC impedance values of lithium-ion cells, obtained from the same lot as the spacecraft batteries, were determined using current pulses at various states of charge and temperatures. The cells were discharged at a nominal rate of ~*C*/6 to the desired state of charge. The cells were then kept in the open circuit condition for a period of 2 h before and after the current pulse, to enable the electrodes to establish true equilibrium conditions. The current pulse used for determining the impedance had a magnitude of 4 A and a duration of 60 s. For example, Fig. 1 shows the typical responses of a cell, both upon the current-injection and current-interruption method of measuring impedance, at −20 °C.

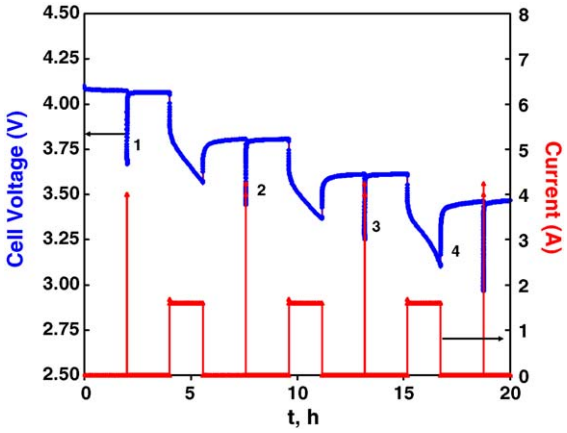

Fig. 1. Measurement of the DC impedance of a 10 Ah Mars Exploration Rover Li-ion cell at −20 °C and (1) 100%, (2) 75%, (3) 50% and (4) 25% state of charge, at 4.0 A discharge pulses for 60 s duration with 2 h rest between after discharge.

Fig. 2A–C shows the variation of the DC cell impedance with state of charge, at three different temperatures, 25, 0 and −20 °C, respectively. As may be seen from these figures, the cell impedance exhibits a parabolic shape, on expanded scale, as a function of state of charge, with the lowest impedance around 50% state of charge and relatively high impedance at either ends, i.e., fully charged or fully discharged states. Also, this shape becomes more pronounced at low temperatures. This may be understood in terms of the kinetics for a reversible process becoming more facile, when the concentrations of the reactants and products are identical, i.e., at 50% state of charge. A similar trend was earlier observed by us [11] and others [12], relative to lithium intercalation kinetics in niobium triselenide and titanium disulfide cathodes, respectively.

An Arrhenius-type plot of the cell DC impedance as a function of temperature is displayed in Fig. 3. Both the actual values of impedance as well as the slope are marginally lower around 50% state of charge, compared to the fully charged (~100% SOC) state or nearly discharged state (~25% SOC). As may be seen from the figure, the cell impedance increases sharply at low temperatures, where the ohmic, charge transfer and mass transfer polarizations are expected to increase at different rates, depending upon the characteristics of each of these processes. However, due to the fact that the pulse durations employed here are rather short (60 s in this; nevertheless, similar trend was observed with shorter pulses of 30 mS duration), it is unlikely to have any significant concentration gradients developed in the electrodes or electrolyte. Contributions from mass transfer may, therefore, be ignored here and the increasing cell impedance may be understood in terms of decreasing electronic and ionic conductivities in the electrode and electrolyte and/or decreasing lithium intercalation kinetics either at the anode/electrolyte or cathode/electrolyte interface.

The effect of charge–discharge cycling on the cell impedance is illustrated in Fig. 4A–D. Fig. 4A shows the capacity retention of MER Li-ion cells during cycling at 23 °C using a discharge rate of *C*/6 (to 3.0 V) and a charge rate of *C*/6 (to 4.1 V, followed by constant–voltage charging until the charge current

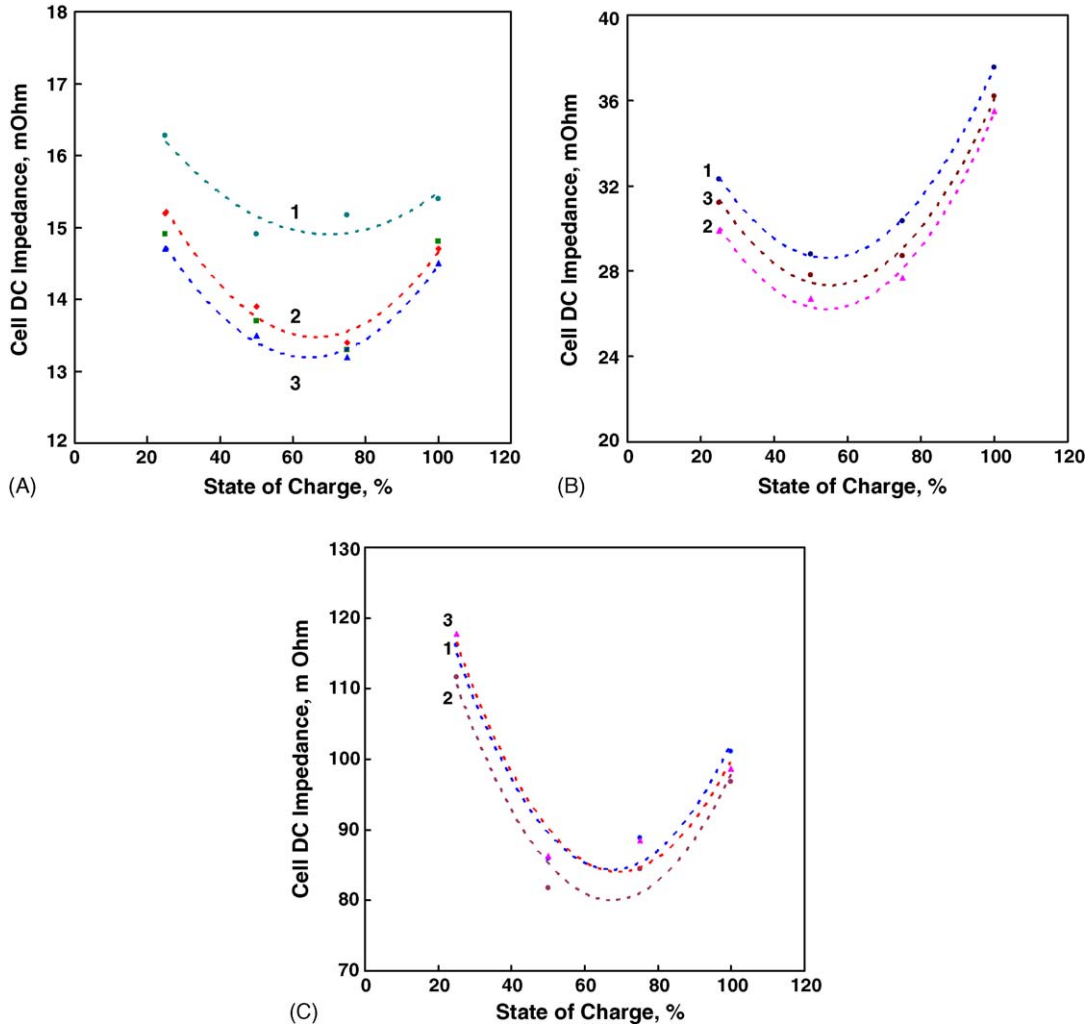

Fig. 2. DC impedance of a 10 Ah Mars Exploration Rover Li-ion cell at (A) 25 °C, (B) 0 °C and (C) −20 °C, as function of state of charge from (1) current injection, and (2) 5 and (3) 120 min after current interruption.

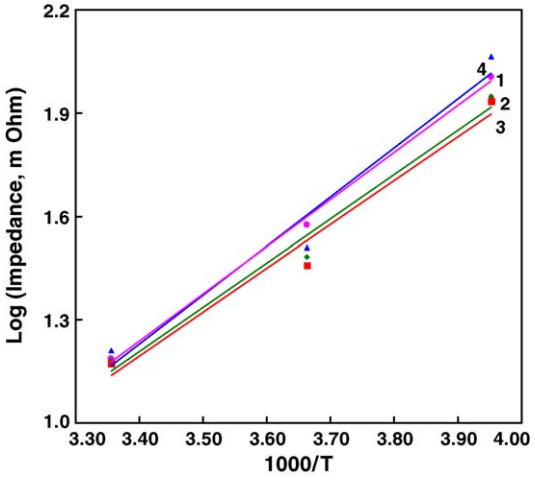

Fig. 3. Arrhenius plots of the DC impedance of a 10 Ah Mars Exploration Rover Li-ion cell at (1) 100%, (2) 75%, (3) 50% and (4) 25% states of charge.

tapers below *C*/50). As may be seen from the figure, the MER Li-ion cell displays good cycling behavior, retaining nearly 80% of the initial capacity after 1000 deep-discharge (100% DOD) cycles. The DC impedance measurements performed at 23 °C on this cell, both at 100% and 50% states of charge, and at various stages of cycling are shown in Fig. 4B and C, respectively. As may be seen from these figures, the voltage drop upon pulsing continues to increase during cycling. In other words, the polarization or impedance increases during cycling, almost linearly with increasing cycle number (Fig. 4D). Once again, the slope, as well as the actual values of impedance, are marginally higher at 100% state of charge, compared to 50% state of charge. The impedance increase is about 5.5 and 5.0 mΩ per 100 cycles at 100% and 50% state of charge, respectively. A similar increase in the DC impedance has also been observed during storage, which is not being presented here. This increase in impedance, either during electrochemical cycling or storage, is primarily a result of the build-up of surface films on the electrodes [13–15], termed as solid electrolyte interface films (SEI) [16], typically present on the anode and also claimed to exist on the cathode [17], and/or a decrease in the interfacial conditions to inhibit lithium intercalation process.

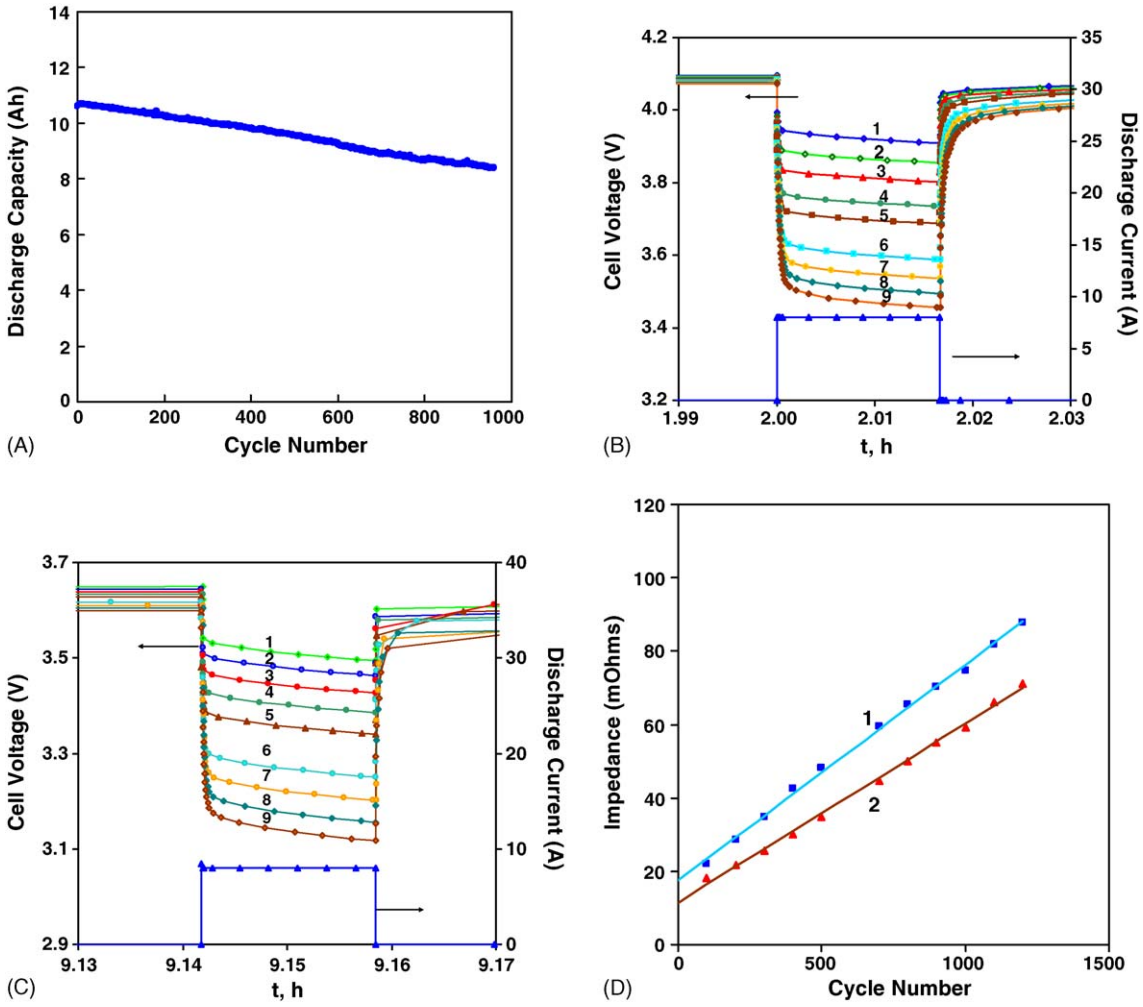

Fig. 4. Effect of charge–discharge cycling on the DC impedance of MER Li-ion cell: (A) capacity retention during cycling to 100% DOD at 20 °C, at a discharge current of *C*/6 to 3.0 V and charge rate of *C*/6 to 4.1, followed by tapered charge to *C*/50, (B) DC impedance, with 8 A pulse for 60 s, at 100 % state of charge after (1) 100, (2) 200, (3) 300, (4) 400, (5) 500, (6) 640, (7) 740, (8) 840 and (9) 940 cycles, (C) DC impedance at 50% state of charge, after cycling as above, and (D) variation of DC impedance at (1) 100% and (2) 50% states of charge during charge–discharge cycling as above.

4.1.1. DC current pulse magnitude

The impedances of the cells were also measured using different DC current pulses and at different temperatures. This is mainly to ascertain the effect of pulse magnitude on the measured value of the cell or battery impedance and also to identify the optimum pulse current that will provide realistic and meaningful values for the impedance. As expressed in Eq. (2), the impedance is a strong function of the current, mainly due to the charge transfer polarization decreasing with increasing current. Both the ohmic and mass transfer polarizations are expected to be invariant with the pulse current, unless the duration is long enough to cause significant concentration gradients or changes in the state of charge and hence the material properties. Fig. 5A shows the effect of pulse magnitude on the cell impedance, at 20 °C and at different states of charge. Fig. 5B–E illustrates similar effects at 0, −20, −30 and −40 °C, respectively. As may be seen from these figures, the impedance decreases with increasing pulse magnitude, at all states of charge, due to decreasing contributions from charge transfer polarization. Typically, the decrease in the impedance with increasing current is more noticeable at low states of charge. Furthermore, these differences are more significant at lower temperatures.

4.1.2. DC current pulse duration

Another variable for the impedance measurements, using DC current pulses, is pulse duration. The objective here is, once again, is to ascertain the effect of pulse magnitude on the measured values of cell or battery impedance and also to identify optimum range of pulse duration that would provide realistic and meaningful values for the impedance for a given application. As expressed by the rate equation (2), the impedance varies significantly with the pulse width. Short pulses will be useful to minimize the cell impedance, due to reduced contributions from mass transfer. Long-duration pulses, on the other hand, will result in considerable concentration gradients and hence mass transfer polarization, especially at low temperatures.

Fig. 6A shows the sequence of measurements performed at different currents, pulse durations and states of charge, at different temperatures, e.g., at −20 °C. For instance, pulse measurements were performed as a function of the pulse magnitude

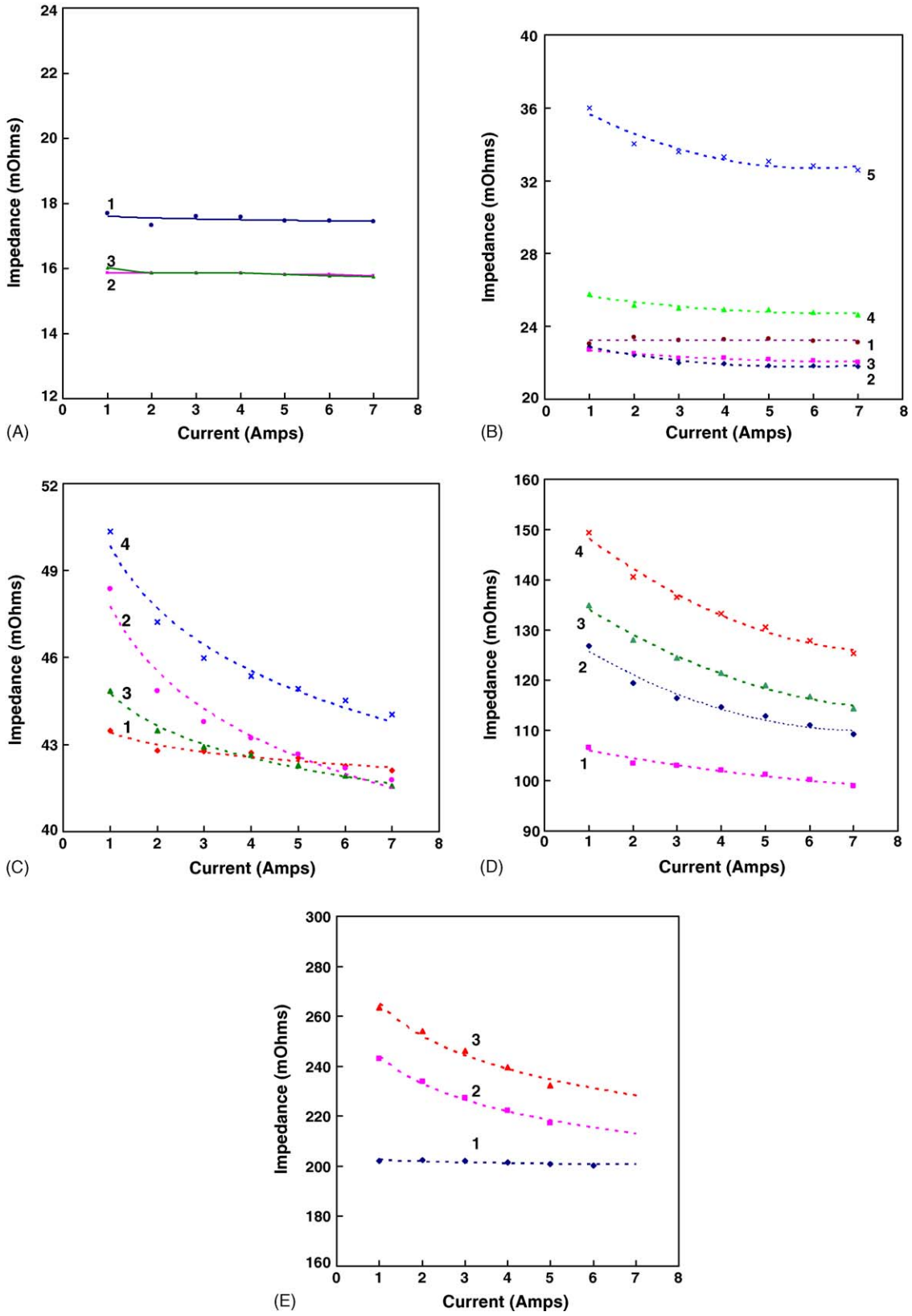

Fig. 5. DC impedance of a 10 Ah Mars Exploration Rover Li-ion cell, as a function of the magnitude of the pulse at (1) 100%, (2) 75%, (3) 50% and (4) 25% state of charge, and at: (A) 20 °C, (B) 0 °C, (C) −20 °C, (D) −30 °C and (E) −40 °C.

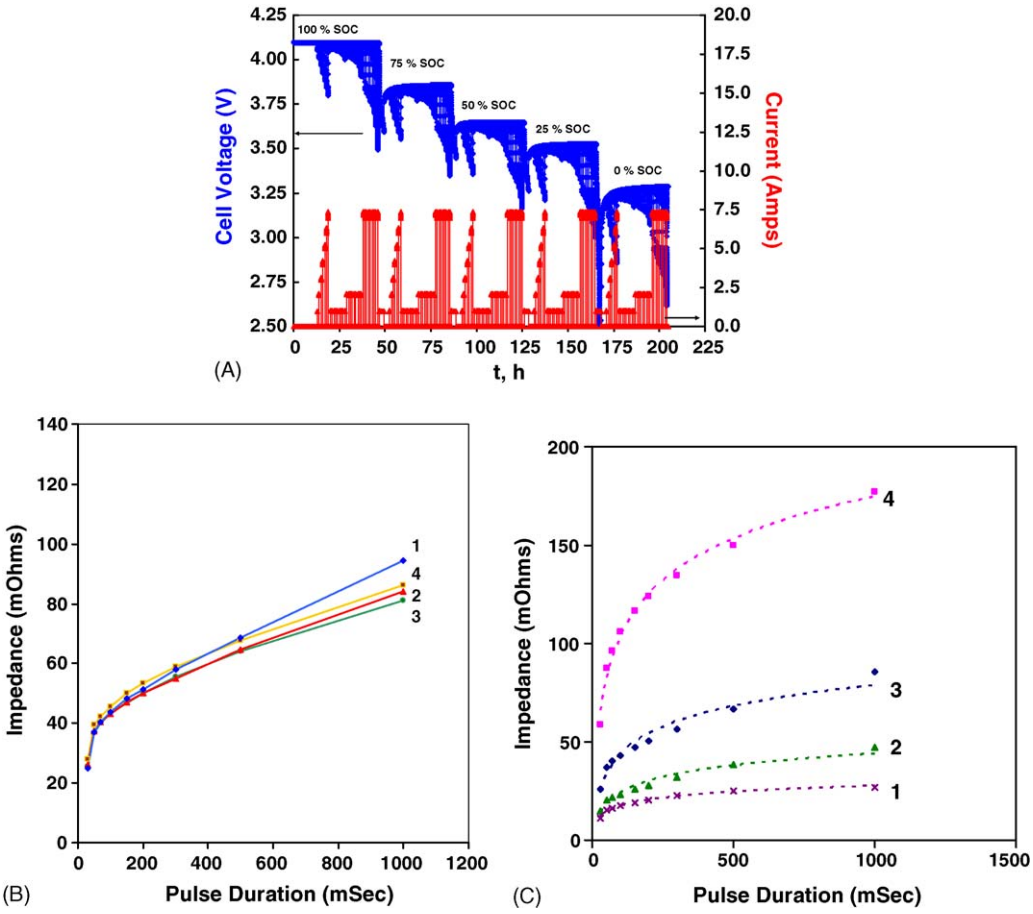

Fig. 6. Effect of pulse duration on the DC impedance of a MER Li-ion cell: (A) impedance determination at different states of charge, at different pulse current currents and durations, at −20 °C, (B) increase in the DC impedance at 1 A with the pulse duration at: (1) 100%, (2) 75%, (3) 50% and (4) 25% states of charge at −20 °C, (C) variation of DC impedance, measured at 7 A, with pulse duration at 100% state of charge and at (1) 20 °C, (2) 0 °C, (3) −20 °C and (4) −30 °C.

from 1 to 7 A. These measurements were followed by pulses with different pulse magnitudes, from 30 ms to 1 s at 1, 2 and 7 A. We performed similar sets of measurements at different states of charge, i.e., at 100%, 75%, 50%, 25 and 0%, wherever possible, and at temperatures of 20, 0, −20, −30 and −40 °C.

The variation of cell impedance with pulse duration at different states of charge, for example at −20 °C, is illustrated in Fig. 6B. Expectedly, with increasing pulse duration, the impedance increases, as a result of increased mass transfer polarization. State of charge does not seem to have noticeable impact on the contribution of the mass transfer polarization. Temperature, on the other hand, has more significant impact on the impedance, especially when measured using long pulses (Fig. 6C). With a decrease in temperature, the increase in the mass transfer polarization during long pulses is more dramatic, owing to a reduction in the mass transfer kinetics.

5. Discussion

As described above, the impedance is comprised of three components, i.e., ohmic, charge transfer and mass transfer polarizations. However, under the appropriate conditions, the impedance can be successfully resolved into component contributions, yielding valuable information.

5.1. Pulse magnitude

The impedance, obtained from short DC pulses, of the order of mS, will essentially contain the ohmic and charge transfer components, with no contribution from the mass transfer process. The electrochemical rate equation (Eq. (2)) can be simplified, under these conditions, as

$$\frac{i}{i_0} = \left[\exp\left(-\frac{\alpha n F}{RT}\eta\right) - \exp\left(\frac{(1-\alpha)nF}{RT}\eta\right)\right] \tag{3}$$

At sufficiently high currents, the corresponding overpotentials are high enough, that the reaction is in the Tafel regime, i.e., the reverse electrochemical reaction can be ignored. Assuming that both the rate determining processes, which in this case could be either the anode half-reaction or the cathodic process are in the Tafel regime, it can be expressed, as

$$\eta_{\mathrm{Ch}} = -\frac{RT}{\alpha n F}\ln\left(\frac{i}{i_0}\right) \tag{4}$$

Thus, the total polarization is

$$\eta = iR_{\mathrm{Ohm}} - \frac{RT}{\alpha n F}\ln\left(\frac{i}{i_0}\right) \tag{5}$$

which upon differentiation yields:

$$\frac{\partial \eta}{\partial i} = R_{\text{Ohm}} - \frac{2.303RT}{\alpha n F}\left(\frac{1}{i}\right) \quad (6)$$

A plot of the cell impedance as a function of reciprocal of current will thus be linear with a slope corresponding to the Tafel coefficient and intercept corresponding to the ohmic resistance.

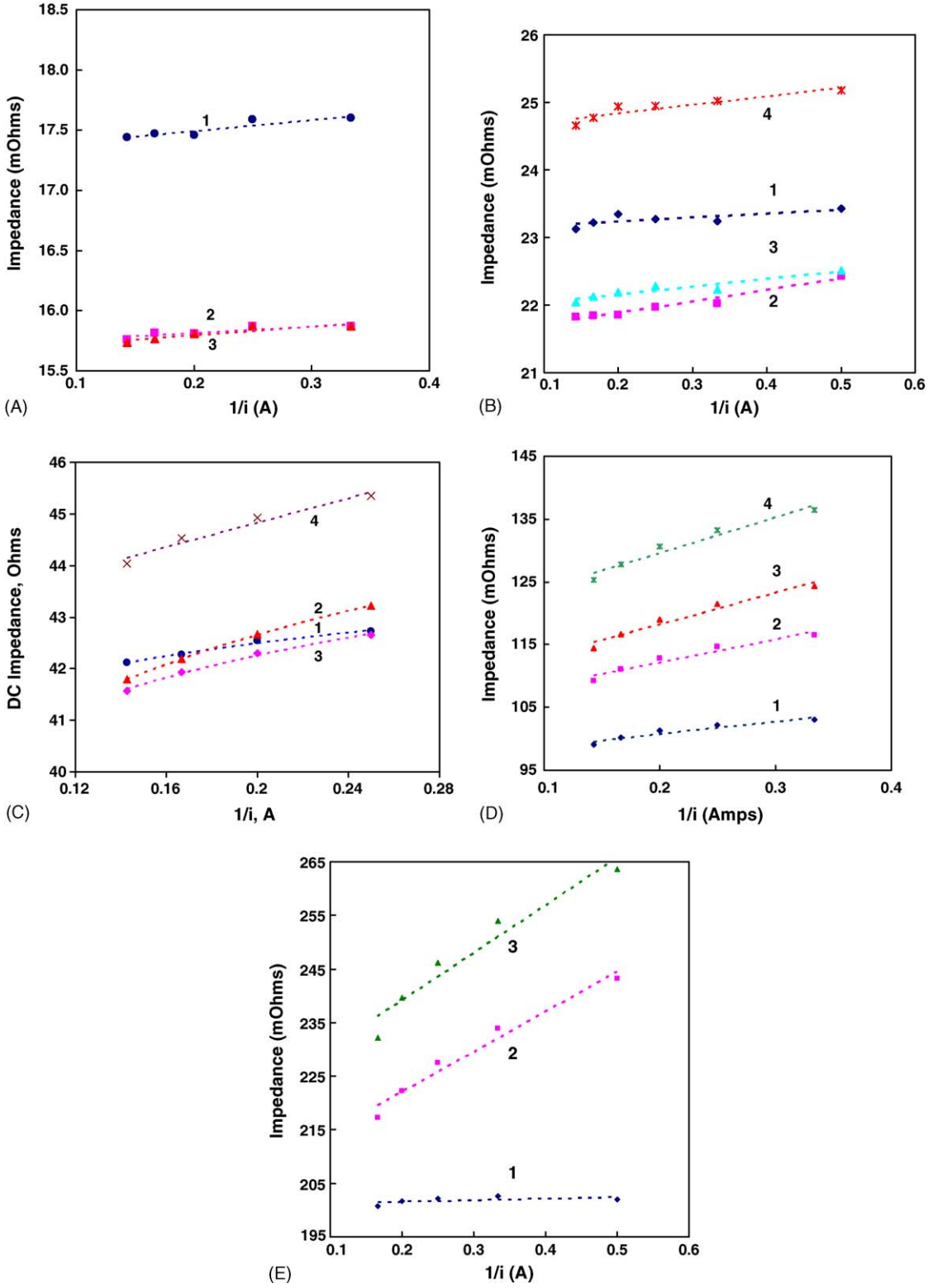

Fig. 7. Effect of pulse current on the DC impedance of a MER 10 Ah Li-ion cells: variation of impedance with 1/*I* at (A) 20 °C, (B) 0 °C, (C) −20 °C, (D) −30 °C and (E) −40 °C and at (1) 100%, (2) 75%, (3) 50% and (4) 25% state of charge.

Fig. 7A shows the variation of the expected linear dependence of the impedance with the reciprocal of the pulse magnitude at three different states of charge at 20 °C. As may be expected from Eq. (6), the impedance shows a linear dependence, increasing linearly with a decrease in the reciprocal current. Similar curves at other temperatures, i.e., 0, −20, −30 and −40 °C are shown in Fig. 7B–E, respectively. The intercepts of these curves provide the values of ohmic polarization of the cell at various states of charge and temperature, while the slopes allow us to calculate the Tafel slopes under these conditions. The charge transfer contribution is obtained by subtracting the ohmic component from the total impedance. Fig. 8A illustrates the variation of ohmic impedance as well as charge transfer resistance (with a pulse magnitude of 2 A), at different temperatures. Both the ohmic as well as the charge transfer components increase at low temperatures. However, their relative contributions also change with temperature. For example, the contribution from ohmic polarization decreases from about 98–99% at 20 °C to about 82% at −40 °C, whereas the charge transfer component increases from 1–2% at 20 °C to about 18% at −40 °C (Fig. 8B). These ratios will, however, change depending on the pulse current. A low pulse current would decrease the ohmic component, while a higher current pulse would increase its share.

It is interesting to note that the ohmic polarization constitutes a significant portion of the cell impedance at ambient as well as at low temperatures. It is therefore imperative that more conductive electrolytes, current collectors, conductive diluents and/or thin-porous separators are deemed essential for minimizing the cell impedance, and thus, achieving higher power densities.

The Arrhenius-type plots of the ohmic and charge transfer polarizations are depicted in Fig. 8C, at two different states of charge. Again, the state of charge seems be a non-factor, while the slopes for the ohmic and charge transfer impedances are substantially different. Further, the slope for the charge transfer kinetics is about twice as large (2.6 versus 1.2), compared to the ohmic resistance, implying that the charge transfer (kinetic) process is hindered more at low temperatures, compared to the ionic conduction process. The activation energies calculated for the processes related to ohmic polarization and charge transfer polarization, i.e., ionic conduction and electron transfer, are 6.03 and 12.53 kcal mol^{-1} K^{-1}, respectively.

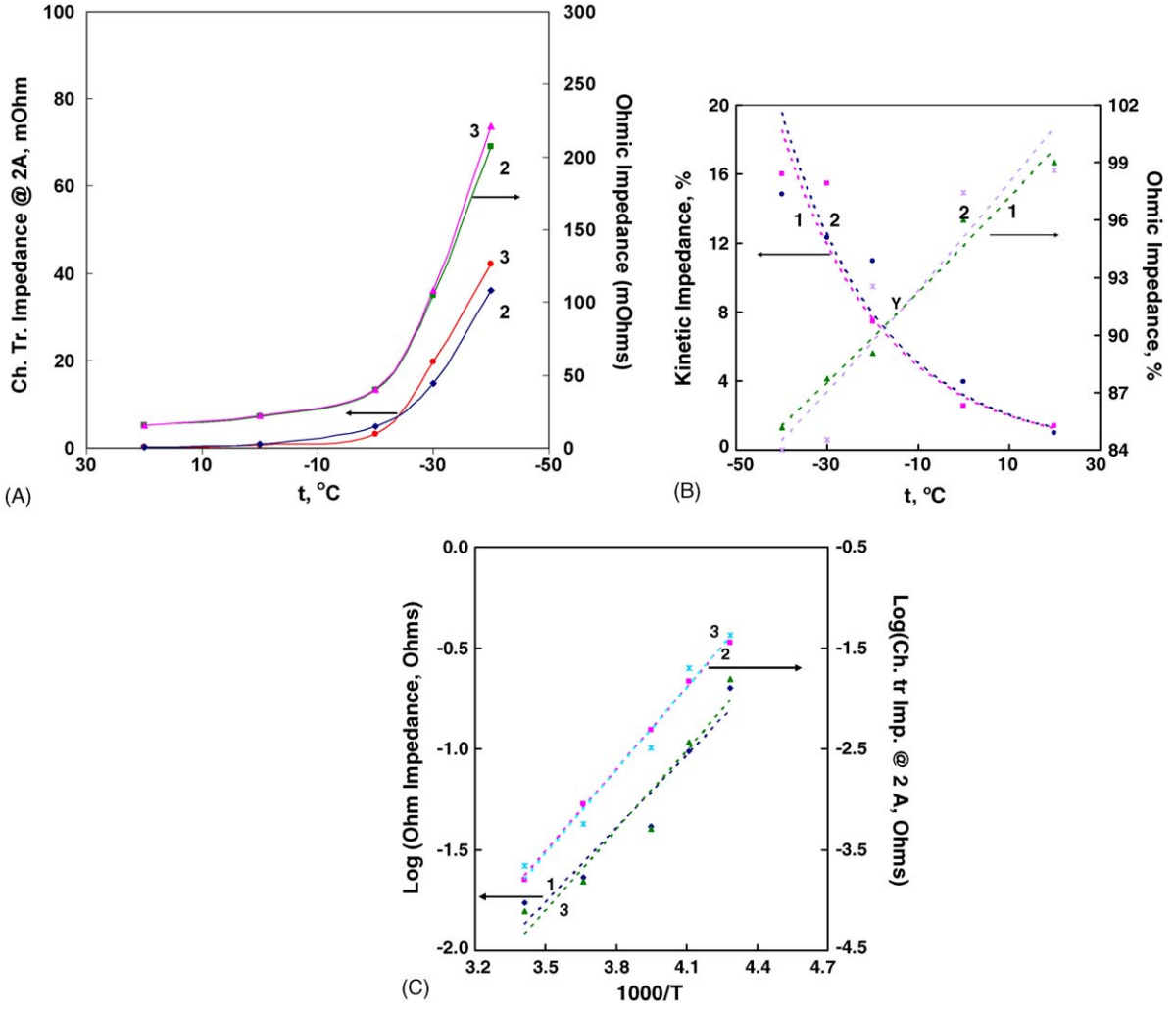

Fig. 8. Effect of pulse current on the DC impedance of MER 10 Ah Li-ion cells: (A) variation of ohmic and charge transfer polarization with temperature, and (B) relative proportions of ohmic and charge transfer components as a function of temperature and (C) Arrehenius plots of ohmic and charge transfer components of the DC impedance at (1) 100%, (2) 75% and (3) 50% state of charge.

5.2. Pulse duration

The limiting current, i_l, under steady-state, convective–diffusion conditions may be expressed as [18]:

$$i_l = \frac{nFAD}{\delta} C_O \quad (7)$$

where D is the diffusion coefficient, A the area of the electrode, n the number of electrons involved in the rate determining step, F the Faraday constant, C_O the bulk concentration of the reactant and δ is the thickness of the boundary layer.

In the case of a lithium-ion cell, it is reasonable to assume that there is no convection. Even the natural convection arising out of density gradients is absent because of invariance of the electrolyte density during charge and discharge. Under purely diffusion-limited conditions, there would not be anything like a steady-state condition. Instead, the boundary layer continues to grow at a rate proportional to $t^{0.5}$. In other words, the current decreases at a rate proportional to $t^{0.5}$. Alternately, the impedance increases with time at a rate proportional to $t^{0.5}$.

A plot of the impedance against $t^{0.5}$ would thus be linear, with a slope containing diffusion coefficient, along with several other constants. Fig. 9A shows such a plot for the 10 Ah Li-ion cell at various temperatures. It is clear from these plots, that the impedance does increase linearly with $t^{0.5}$ and the increase is more significant as the temperature is decreased. The latter is expected in view of the slower diffusional kinetics at low temperatures. From the Arrhenius plot of the above slopes against inverse temperatures, the activation energies for the diffusion process are estimated to be 8.74 and 11.76 kJ mol^{-1}, for 100% and 75% state of charge, respectively. Thus, it is possible to estimate the activation energies for the rate controlling diffusional process in a two-terminal Li-ion cell, using the DC current pulses of different pulse duration, even though it is not possible to determine the actual value of the diffusion coefficient in the individual electrodes.

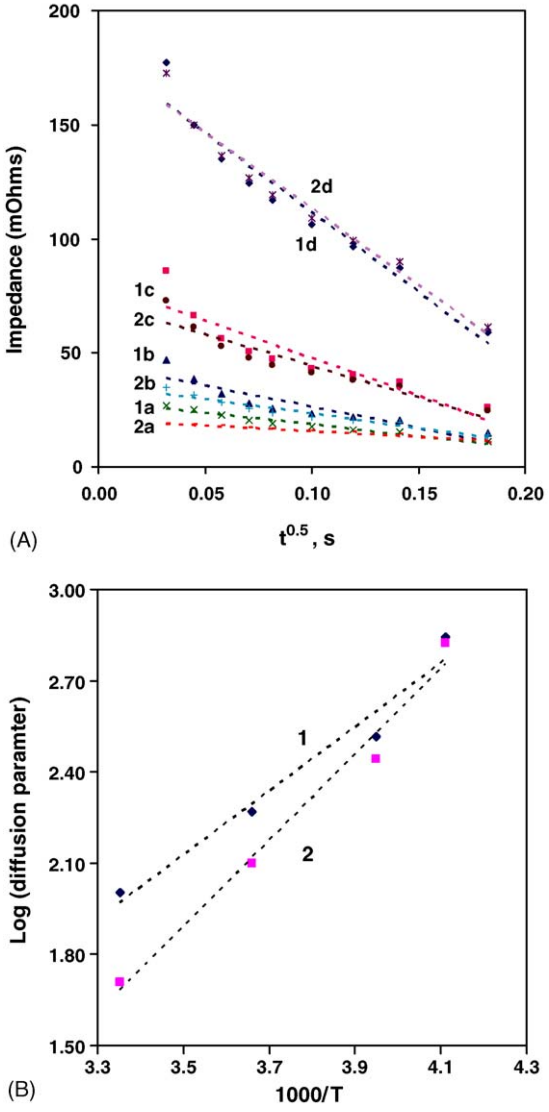

Fig. 9. Effect of pulse duration on the DC impedance of MER 10 Ah Li-ion cells: (A) variation of DC impedance with $t^{0.5}$ at (1) 100% and (2) 75% state of charge and at (a) 20 °C, (b) 0 °C, (c) −20 °C and (d) −30 °C. (B) Arrehenius plots of diffusion-related parameter at (1) 100% and (2) 50% state of charge.

5.3. Impedance of Mars Exploration Rover batteries-launch dilemma

The DC impedance of the rover mission-simulation (or engineering) batteries displayed values of 123, 251 and 606 mΩ, with a sampling current of 5A for a 60 s duration, at 20, 0, and −20 °C, respectively. When we increased the sampling current to 30 A for a short-duration of 50 mS, we found the impedance values decreased to 104 and 133 mΩ at 0 and −10 °C, respectively. From a set of systematic measurements at −18 °C, we determined that the battery impedance drops continuously from a high value of over 900 mΩ at 250 mA to about 500 mΩ at 5 A.

This trend of lower impedance at high sampling currents is consistent with the cell behavior, described in the previous sections. The ohmic polarization of the battery, estimated from the intercept of the impedance against the reciprocal of current (Fig. 10A), is around 191 mΩ at −16 °C. This corresponds to a cell impedance of 23.8 mΩ. From the impedance measurements made with pulses of different durations, we estimated the diffusion parameter corresponding to the rate-determining electrode, i.e., the slope of impedance against $t^{-0.5}$ (Fig. 10B), to be around 2000 mΩ, which corresponds well with the cell value of 328 mΩ at −20 °C.

Finally, there was some uncertainty in these measurements due to the slow data acquisition rate by the Maccor battery system we used. The system typically averages over eight data points, at the rapid acquisition rate of one point each 10 mS. To resolve this uncertainty, the impedance of rover batteries was measured using an oscilloscope for rapid data acquisition at 5, 11 and 17 A. Fig. 10C shows such an oscilloscopic trace of the rover battery. As may be seen here, there are no undershoots in the battery voltage even in mS range and the battery impedances were 260 mΩ, 263 mΩ, and 287 Ω, at 5, 11, and 17 A, respectively. They are within the range that may be expected from the cell values.

From the mission standpoint, these values for the rover batteries were perceived to be high enough to have not thermally

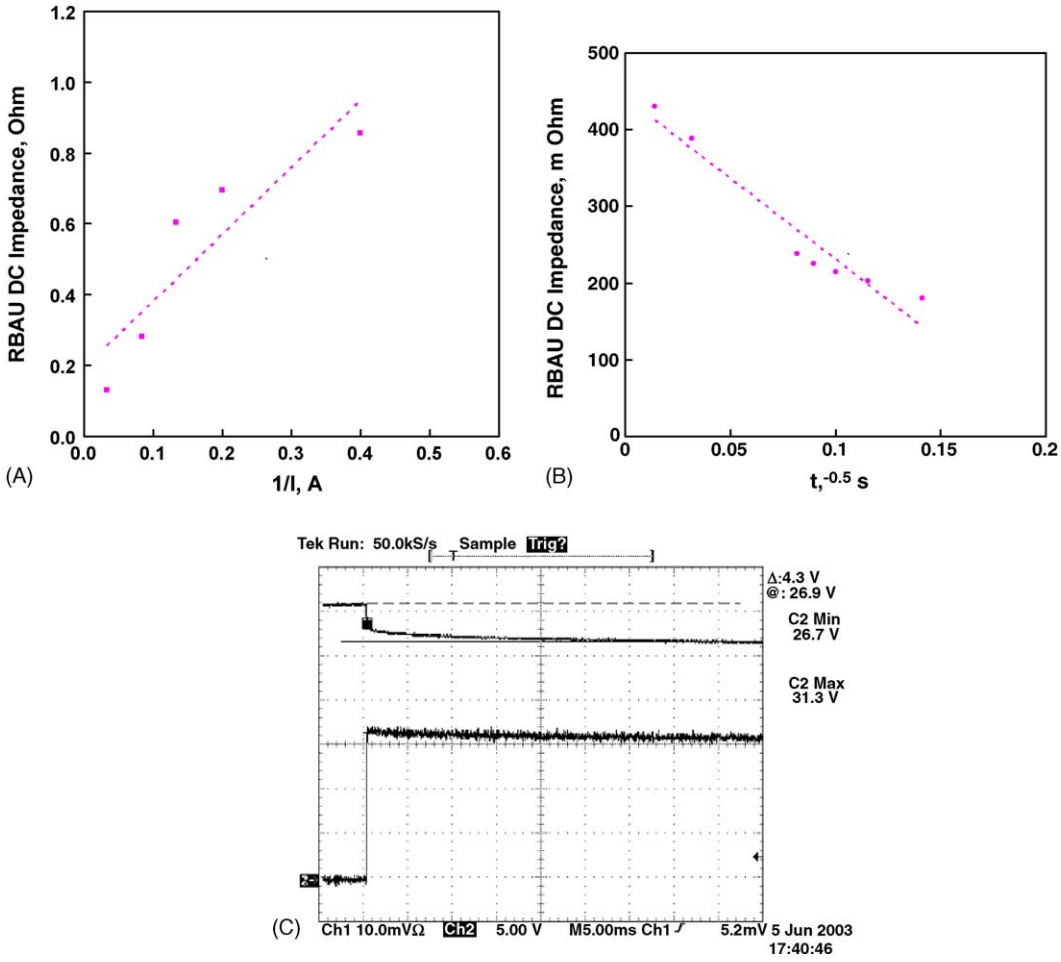

Fig. 10. DC impedance of MER Li-ion battery at −20 °C: (A) effect of pulse current on the DC impedance, (B) effect of pulse duration at 12 A and (C) oscilloscope trace with rapid data capture.

stressed the series resistor in the event of squib plasma, especially since the spacecraft temperatures would be a couple of degrees lower than −16 °C, i.e., close to −18 °C. Accordingly, it was determined to be an acceptable risk to proceed with the launch, without having to replace the current limiting resistors.

6. Conclusions

Despite the fact that AC impedance methods of determining the cell impedance are rather sophisticated and elegant to provide detailed information on individual components of ohmic, charge transfer and mass transfer polarizations from a single experiment, they are often plagued by the complexity both in the experimentation as well as interpretation of the data, especially in a two-terminal device or without a reference electrode. The DC pulse method, on the other hand, is easier to implement and can provide useful information on individual components of cell and battery impedances with judicious experiments at different pulse magnitudes and pulse durations, as demonstrated here. Short DC pulses of different magnitudes enabled the separation of kinetic and ohmic components. Interestingly, the ohmic polarization continued to be a dominant component even at low temperatures, even though the proportion of the charge transfer component was observed to increase at low temperatures. From the measurements with pulses of different durations, we estimated the activation energies for the rate-limiting diffusion process, either in the anode or cathode. The simplicity of this method makes it attractive for determining similar characteristics in a multi-cell battery. These studies underline the need to adopt similar pulse conditions for impedance determination, as in the desired application, to make the impedance values realistic and useful. Finally, this method was successfully applied to the Li-ion batteries on the Mars Exploration Rovers to make a proper assessment of the risk associated with the series current-limiting resistor, prior to the launch of the spacecraft.

Acknowledgements

The work described here was carried out at the Jet Propulsion Laboratory, California Institute of Technology, for the Mars Exploration Rover Project, under contract with the National Aeronautics and Space Administration (NASA). The cells and batteries for this study were fabricated by Lithion, Inc. (Yardney Technical Products). We thank the following JPLers: Drs. John Klein, Joseph Savino from the MER team and S.R.

Narayanan and Harvey Frank from the Electrochemical Technologies Group for their stimulating discussions and suggestions.

References

[1] B.V. Ratnakumar, M.C. Smart, R.C. Ewell, L.D. Whitcanack, A. Kindler, K.B. Chin, S.R. Narayanan, S. Surampudi, Li-ion and Li primary batteries on spirit and opportunity Mars Rovers, in: Proceedings of the 12th International Meeting on Lithium Batteries (IMLB), June 27–July 2, 2004.

[2] B.V. Ratnakumar, M.C. Smart, A. Kindler, H. Frank, R. Ewell, S. Surampudi, Lithium batteries for aerospace applications: 2003 Mars Exploration Rover, J. Power Sources 119–121 (2003) 906–910.

[3] B.V. Ratnakumar, M.C. Smart, R.C. Ewell, L.D. Whitcanack, K.B. Chin, S.R. Narayanan, S. Surampudi, Our experiences with lithium batteries on Mars Exploration Rovers, in: Space Power Workshop, Manhattan Beach, CA, April 19–22, 2004.

[4] M.C. Smart, B.V. Ratnakumar, S. Surampudi, Electrolytes for low-temperature lithium batteries based on ternary mixtures of aliphatic carbonates, J. Electrochem. Soc. 146 (2) (1999) 486–492.

[5] M.C. Smart, B.V. Ratnakumar, L.D. Whitcanack, K.B. Chin, M.D. Rodriguez, S. Surampudi, Performance characteristics of lithium-ion cells for NASA's Mars 2001 Lander application, IEEE Aerospace Electron. Syst. Mag. 14 (11) (1999) 36–42.

[6] J. Allen, Bard, R. Larry, Faulkner, Electrochemical Methods: Fundamentals and Applications, Wiley, New York, 1980.

[7] J. Ross Macdonald (Ed.), Impedance Spectroscopy: Emphasizing Solid Materials and Systems, John Wiley and Sons, New York, 1987.

[8] I. Bloom, A.N. Jansen, D.P. Abraham, J. Knuth, S.A. Jones, V.S. Battaglia, G.L. Henriksen, Differential voltage analyses of high-power, lithium-ion cells. 1. Technique and Application, J. Power Sources 139 (2005) 295–303.

[9] I. Bloom, J. Christophersen, K. Gering, Differential voltage analyses of high-power, lithium-ion cells. 2. Applications, J. Power Sources 139 (2005) 304–313.

[10] R.B. Wright, C.G. Motloch, J.R. Belt, J.P. Christophersen, C.D. Ho, R.A. Richardson, I. Bloom, S.A. Jones, V.S. Battaglia, G.L. Henriksen, T. Unkelhaeuser, D. Ingersoll, H.L. Case, S.A. Rogers, R.A. Sutula, J. Power Sources 110 (2002) 445–470.

[11] B.V. Ratnakumar, S. Di Stefano, C.P. Bankston, AC impedance of niobium triselenide cathode in secondary lithium cells, J. Appl. Electrochem. 19 (6) (1989) 813–818;
B.V. Ratnakumar, S. Di Stefano, C.P. Bankston, AC impedance of niobium triselenide cathode in secondary lithium cells, in: Proceedings of the 33rd Power Sources Conference, Cherry Hill, NJ, June 13–16, 1988.

[12] M.S. Wu, P.C.J. Chiang, J.C. Lin, J. Electrochem. Soc. 152 (1) (2005) A47–A52.

[13] D. Zhang, B.S. Haran, A. Durairajan, R.E. White, Y. Podrazhansky, B.N. Popov, J Power Sources 91 (2000) 122.

[14] M.S. Wu, P.C.J. Chiang, J.C. Lin, J. Electrochem. Soc. 152 (6) (2005) A1041–A1046.

[15] E. Barsoukov, J.H. Kim, J.H. Kim, C.O. Yoon, H. Lee, Solid State Ionics 116 (1999) 249–261.

[16] E. Peled, in: L.J.P. Gabano (Ed.), Lithium Batteries, Academic Press, New York, 1983 (Chapter 3).

[17] B. Markovsky, A. Rodkin, Y.S. Cohen, O. Palchik, E. Levi, D. Aurbach, H.J. Kim, M. Schmidt, J. Power Sources 119 (2003) 504–510.

[18] K.J. Vetter, Electrochemical Kinetics, Academy Press, New York, 1967.